Mon. Not. R. Astron. Soc. **364,** 552–564 (2005) doi:10.1111/j.1365-2966.2005.09574.x

Feedback and metal enrichment in cosmological smoothed particle hydrodynamics simulations – I. A model for chemical enrichment

C. Scannapieco,[1,2⋆] P. B. Tissera,[1,2⋆] S. D. M. White[3⋆] and V. Springel[3⋆]

[1] *Instituto de Astronomía y Física del Espacio, Casilla de Correos 67, Suc. 28, 1428, Buenos Aires, Argentina*
[2] *Consejo Nacional de Investigaciones Científicas y Técnicas, CONICET, Argentina*
[3] *Max-Planck Institute for Astrophysics, Karl-Schwarzchild Str. 1, D85748, Garching, Germany*

Accepted 2005 August 31. Received 2005 August 29; in original form 2005 April 26

ABSTRACT

We discuss a model for treating chemical enrichment by Type II and Type Ia supernova (SNII and SNIa) explosions in simulations of cosmological structure formation. Our model includes metal-dependent radiative cooling and star formation in dense collapsed gas clumps. Metals are returned into the diffuse interstellar medium by star particles using a local smoothed particle hydrodynamics (SPH) smoothing kernel. A variety of chemical abundance patterns in enriched gas arise in our treatment owing to the different yields and lifetimes of SNII and SNIa progenitor stars. In the case of SNII chemical production, we adopt metal-dependent yields. Because of the sensitive dependence of cooling rates on metallicity, enrichment of galactic haloes with metals can in principle significantly alter subsequent gas infall and the build-up of the stellar components. Indeed, in simulations of isolated galaxies we find that a consistent treatment of metal-dependent cooling produces 25 per cent more stars outside the central region than simulations with a primordial cooling function. In the highly enriched central regions, the evolution of baryons is however not affected by metal cooling, because here the gas is always dense enough to cool. A similar situation is found in cosmological simulations because we include no strong feedback processes which could spread metals over large distances and mix them into unenriched diffuse gas. We demonstrate this explicitly with test simulations which adopt suprasolar cooling functions leading to large changes both in the stellar mass and in the metal distributions. We also find that the impact of metallicity on the star formation histories of galaxies may depend on their particular evolutionary history. Our results hence emphasize the importance of feedback processes for interpreting the cosmic metal enrichment.

Key words: methods: numerical – galaxies: abundances – galaxies: evolution – galaxies: formation – cosmology: theory.

1 INTRODUCTION

Over the last decades, our knowledge of the chemical properties of the Universe and, in particular, of galaxies has improved dramatically. Observations of the local Universe (e.g. Garnett & Shields 1987; Skillman, Kennicutt & Hodge 1989; Brodie & Huchra 1991; Zaritsky, Kennicutt & Huchra 1994; Mushotzky et al. 1996; Ettori et al. 2002; Tremonti et al. 2004; Lamareille et al. 2004) as well as at intermediate and high redshifts (e.g. Prochaska & Wolfe 2002; Adelberger et al. 2003; Kobulnicky et al. 2003; Lilly, Carollo & Stockton 2003; Shapley et al. 2004) have resulted in a quite detailed picture of the chemical history of the stellar populations and of the interstellar and intergalactic media. It is an important challenge for the theory of galaxy formation to explain these observational results in the context of the current cosmological paradigm. Numerical simulations are an important tool to make specific predictions for galaxy formation theories and to confront them with observations, because they can accurately track the growth of structure in the dark matter and baryonic components. It is hence natural to ask what such simulations predict for the chemical properties of the Universe.

Currently, hydrodynamic cosmological simulations including radiative cooling and star formation, at best, coarsely reproduce the observed properties of galaxies. They fail when scrutinized in detail. Among the most prominent problems are 'catastrophic angular momentum loss' (e.g. Navarro & Benz 1991; Navarro & White 1994) and the difficulty in finding a consistent modelling of supernova (SN) feedback (e.g. Navarro & White 1993; Metzler & Evrard 1994; Yepes et al. 1997; Marri & White 2003; Springel & Hernquist 2003, hereafter SH03). The first issue mainly affects galaxy

⋆E-mail: cecilia@iafe.uba.ar (CS); patricia@iafe.uba.ar (PBT); swhite@mpa-garching.mpg.de (SDMW); volker@mpa-garching.mpg.de (VS)

morphology, size and kinematics, while the latter primarily influences the efficiency of star formation. Both are the subject of intense research. Reproducing the chemical properties of observed galaxies in detail may be viewed as an intertwined third problem.

Regarding the angular momentum problem, recent simulations have shown some promising advances. Domínguez-Tenreiro, Tissera & Sáiz (1998) found that the formation of compact stellar bulges can stabilize the discs and thereby prevent the angular momentum loss during violent minor merger events, such that disc systems that resemble observed galaxies are obtained. Abadi et al. (2003) have also demonstrated the importance of a dense, slowly rotating spheroidal component, and pointed out its relevance for comparing simulated and observed galaxies consistently. More recently, Robertson et al. (2004) were able to produce large, stable disc systems in their cosmological simulations which are comparable in size to spiral galaxies. In their approach, they introduced a subresolution model for star formation and feedback which pressurizes the star-forming gas and stabilizes discs against fragmentation. We note that all these studies agree on the need for a self-consistent treatment of SN feedback as a crucial mechanism to regulate star formation and to reproduce discs similar to observational counterparts.

SN explosions are thought to play a fundamental role in the evolution of galaxies because they are considered the most efficient and ubiquitous mechanism for the ejection of metals and energy into the interstellar medium (ISM). Both chemical and energy feedback can affect the condensation of gas and consequently the evolution of galactic systems. On one hand, the presence of metals in the ISM affects gas cooling times because the radiative cooling rate depends sensitively on metallicity (Sutherland & Dopita 1993, hereafter SD93). On the other hand, the release of energy is crucial for regulating star formation through the heating and disruption of cold gas clouds, and for producing outflows which can transport enriched material into the intergalactic medium (e.g. Lehnert & Heckman 1996; Dahlem, Weaver & Heckman 1998; Frye, Broadhurst & Benítez 2002; Rupke, Veilleux & Sanders 2002; Martin 2004). As suggested by observations and theory, the largest outflows (e.g. Larson 1974; White & Rees 1978; Dekel & Silk 1986; White & Frenk 1991) should be able to develop in small systems because of their shallower potential wells. Because in hierarchical galaxy formation scenarios large systems are formed by the aggregation of smaller systems, energy feedback from SNe is then expected to have important effects for nearly all systems in the different stages of galaxy formation.

Modelling of chemical feedback has been addressed already in numerous studies, mostly with the aim to reproduce the chemical properties of certain types of galaxies, or of clusters of galaxies (e.g. Larson 1976; Tinsley & Larson 1979; Burkert & Hensler 1988; White & Frenk 1991; Burkert, Truran & Hensler 1992; Ferrini et al. 1992; Theis, Burkert & Hensler 1992; Steinmetz & Müller 1994; Kauffmann 1996; Chiappini, Matteucci & Gratton 1997; Kauffmann & Charlot 1998; Boisser & Prantzos 2000; Valdarnini 2003). As first shown by Mosconi et al. (2001), in order to properly model the process of metal enrichment in galaxy formation it is necessary to consider the full cosmological growth of structure in which mergers and interactions have important effects on the star formation process and the dynamical evolution of galaxies (see also Kawata & Gibson 2003; Tornatore et al. 2004; Okamoto et al. 2005).

Perhaps the most fundamental motivation for the relevance of metal enrichment for galaxy formation is based on the fact that the cooling rate of baryons depends on metallicity (SD93). Radiative cooling in turn allows the condensation of gas into dense and cold clouds, which form the reservoir of material available for the formation of stars. As chemical enrichment is a result of star formation, a chemical feedback cycle emerges, in which metals can in principle significantly accelerate the transformation of baryons into stars. In hierarchical scenarios these processes depend significantly on the chemical prescription adopted (Kaellander & Hultman 1998; Kay et al. 2000). These affect galaxy properties such as the luminosity function (White & Frenk 1991). For these reasons, a detailed analysis of the effects of metal-dependent cooling is clearly important for galaxy formation studies. Substantial numerical challenges in simulations of galaxy formation come from the large dynamic range required, and from the multiphase character of the ISM. Gas in very different physical states coexists in the ISM, but the standard formulation of smoothed particle hydrodynamics (SPH; e.g. Gingold & Monaghan 1977; Lucy 1977) is not well suited to deal with this situation. A number of attempts have been made to solve this problem, ranging from an ad hoc decoupling of phases (e.g. Pearce et al. 1999,2001; Marri & White 2003) to simple analytical subresolution models (SH03) that work with an effective equation of state.

Our new model for SN feedback in SPH cosmological simulations has been divided into two stages: chemical and energy feedback. In this work we address the description of the chemical feedback, which is based on the previous model of Mosconi et al. (2001). In a forthcoming paper, we will present the second part of this work: the implementation of energy feedback in the framework of a multiphase scheme for the ISM, which extends the approach of Marri & White (2003). While a treatment of chemical enrichment without energy feedback is an incomplete picture, we think the complexity of the problem merits a step-wise discussion of our model such that the primary physical effects can be better understood.

This paper is organized as follows. In Section 2, we summarize the numerical implementation of the chemical model, and in Section 3 we analyse the dependence of the results on numerical resolution and input parameters, using simulations of isolated galaxies. We then study in Section 4 the properties of galaxies formed in cosmological simulations and examine how they depend on the chemical model. Finally, in Section 5 we give our conclusions.

2 NUMERICAL IMPLEMENTATION

Our new model for the production and ejection of chemical elements by SNe is based in part on the approach in Mosconi et al. (2001). We have implemented our scheme in the TreePM/SPH code GADGET-2, an improved version of the public code GADGET (Springel, Yoshida & White 2001), which manifestly conserves energy and entropy where appropriate (Springel & Hernquist 2002). Note that we do not use the multiphase treatment and the feedback model developed by SH03 for this code, but we do include their treatment of ultraviolet (UV) background. Also, we use a different parametrization for star formation, as described in detail below.

Chemical elements are synthesized in stellar interiors and ejected into the ISM by SN explosions. In order to model the production and distribution of metals in the context of the simulations, there are three ingredients we have to consider: the SN rate (i.e. the number of exploding stars per time unit), the chemical yields (i.e. the chemical material ejected in explosions) and the typical lifetimes of stars, which determine the characteristic time of the metal release.

In our model, we include a separate treatment of Type II and Type Ia SNe (SNII and SNIa). These two types of SNe originate from different stellar populations, and have different rates, yields and typical time-scales. We use different yields for SNII and SNIa which, in the case of SNII, are metal-dependent. Hence, we will treat SNII and SNIa separately, owing to the need to model their

different characteristics. For example, SNII produce most of the chemical elements, except for iron, which is mainly produced by SNIa. Another difference between these two types of SN is that SNII are the endpoint of the evolution of massive stars with short lifetimes, in contrast to SNIa, which result from the evolution of binary systems with lifetimes of $\sim$1 Gyr.

We assume that initially gas particles have primordial abundances, $X_{\rm H} = 0.76$ and $Y_{\rm He} = 0.24$, and we consider the enrichment by the following elements, assuming production only by SNII and SNIa: H, ^{4}He, ^{12}C, ^{16}O, ^{24}Mg, ^{28}Si, ^{56}Fe, ^{14}N, ^{20}Ne, ^{32}S, ^{40}Ca and ^{62}Zn. Note that we do not consider nucleosynthesis by intermediate-mass stars. Consequently, we concentrate our analysis on elements such as O or Fe where restricting to SN production may be a good approximation. In the rest of this section, we describe the most important aspects of the chemical model, namely the star formation and cooling prescriptions, and our scheme for the production and ejection of metals.

2.1 Star formation

We assume that gas particles are eligible for star formation if they are denser than a critical value ($\rho > \rho_* = 7.0 \times 10^{-26}$ g cm^{-3}, where ρ denotes gas density) and lie in a convergent flow (div $\boldsymbol{v} < 0$).[1] For these particles, we assume a star formation rate (SFR) per unit volume equal to

$$\dot{\rho}_\star = c\frac{\rho}{\tau_{\rm dyn}}, \tag{1}$$

where c is a star formation efficiency (we adopt $c = 0.1$) and $\tau_{\rm dyn} = 1/\sqrt{4\pi G\rho}$ is the dynamical time of the particle. We base the creation of new stellar particles on the stochastic approach of SH03 (see also Lia, Portinari & Carraro 2002). To this end, each gas particle eligible for star formation in a given time-step is assigned a probability p_* of forming a star particle given by

$$p_* = \frac{m}{m_*}\left[1 - \exp\left(-\frac{c\,\Delta t}{\tau_{\rm dyn}}\right)\right], \tag{2}$$

where Δt is the integration time-step of the code, m is the mass of the gas particle, and m_* is defined as $m_* = m_0/N_{\rm g}$ with m_0 being the original mass of gas particles at the beginning of the simulation and $N_{\rm g}$ a parameter which determines the number of 'generations' of stars formed from a given gas particle (we assume $N_{\rm g} = 2$). If a random number drawn from a uniform distribution in the unit interval is smaller than p_*, we form a new stellar particle of mass m_* and reduce the mass of the gas particle accordingly. Once the gas particle mass has become smaller than $m_0/N_{\rm g}$, we instead turn it into a star particle. Newly born stars are assumed to have the same element abundances as the gas mass from which they form.

The main advantage of this stochastic approach is that all particles are either purely stellar or purely gas, which avoids the use of 'hybrid' particles with both gaseous and stellar components. The latter would artificially force the stellar component to evolve dissipately like the gas. Note that, as a consequence of the star formation scheme, the number of baryonic particles in the simulation does not remain constant. Unlike SH03, we also exchange the masses of heavy elements explicitly between gas and star particles. As a result, the mass spectrum of stellar and gas particles is slightly washed out around otherwise sharp discrete values.

[1] See Okamoto et al. (2005) for a different approach.

2.2 Chemical production and distribution

Our numerical implementation of the enrichment model has three main components: SNII element production, SNIa element production and metal distribution.

SNII element production

In order to estimate the SNII rate we use a Salpeter initial mass function (IMF) with lower and upper mass cut-offs of 0.1 and 40 $M_\odot$, respectively, and assume that stars more massive than 8 $M_\odot$ end their lives as SNII. For the chemical production, we adopt the yields of Woosley & Weaver (1995). These are metal-dependent yields and vary differently for different elements. We use half of the iron yield of Woosley & Weaver (1995), as it is often adopted (e.g. Timmes, Woosley & Weaver 1995). For the sake of simplicity, in most of our simulations we have assumed that SNII explode (i.e. produce and eject the chemical elements) within an integration time-step of the code (which is typically $\leqslant 10^6$ yr), because SNII originate in massive stars which have very short characteristic lifetimes of the order of 10^7 yr. However, we have also analysed the effect of relaxing this instantaneous recycling approximation (IRA) for SNII (see Section 3.2).

SNIa element production

As a progenitor model, we adopt the W7 model of Thielemann, Nomoto & Hashimoto (1993), which assumes that SNIa explosions originate from CO white dwarf systems in which mass is transferred from the secondary to the primary star until the Chandrasekhar mass is exceeded and an explosion is triggered. It is generally assumed that the lifetime of such a binary system is in the range $\tau_{\rm SNIa} = [0.1, 1]$ Gyr, depending on the age of the secondary star (Greggio 1996). In our model, the material produced by a SNIa event is ejected when a time $\tau_{\rm SNIa}$ after the formation of the exploding star has elapsed. We choose this time randomly within a given range (in most of our experiments we assume $\tau_{\rm SNIa} = [0.1, 1]$ Gyr). In order to estimate the number of SNIa, we adopt an observationally motivated range for the relative ratio of SNII and SNIa rates (e.g. van den Bergh 1991). We use the chemical yields of Thielemann et al. (1993) for the metal production itself.

Metal distribution

We distribute chemical elements ejected in SN explosions within the gaseous neighbours of exploding star particles, using the usual SPH kernel interpolation technique (Mosconi et al. 2001). Each neighbouring gas particle receives a fraction of the ejected metals according to its kernel weight. For this purpose, gas particle neighbours of stellar particles are identified whenever metal distribution has to take place, and smoothing lengths for these stars are calculated by setting a desired number of gas neighbours that should be enclosed in the smoothing length (we have assumed the same criterium used for the smoothing lengths of gas particles). This is particularly important for the enrichment by SNIa because of the time delay between the formation of the stars and the ejection of metals. Note that after a star particle is created, it is only subject to gravitational forces, unlike the gas particles, which continue to be subject to hydrodynamical forces as well. Consequently, as the system evolves, star particles can release metals associated with SNIa explosions in a different environment from where they were born. This, together with the different lifetimes and yields of SNII explosions, can then produce non-trivial variations in abundance ratios.

2.3 Gas cooling

It is well known that the cooling rate of thin astrophysical plasmas depends sensitively on metallicity, in such a way that at a given density, the cooling rate is higher for a higher metallicity. In Fig. 1 we show the cooling function computed by SD93 from primordial (i.e. no heavy elements) to suprasolar abundance ([Fe/H] = +0.5). As one can see from this figure, the cooling function can show very large variations with the metal abundance of the gas, depending on the temperature range considered. For example, the usual estimates of the cooling time ($\tau_{\rm cool}$) for a gas particle at the critical density (ρ_*) and at a temperature of $T_* = 4 \times 10^4$ K yield that $\tau_{\rm cool}$ is 50 times larger for primordial gas than for a mildly suprasolar medium ([Fe/H] =0.5), 18 times larger than that of a solar abundance one, and still twice as large as the corresponding time for gas with [Fe/H] =−1.5. The temperature range of [10^5–10^6] K shows the largest differences, right in the temperature range relevant to the abundant population of dwarf galaxies.

Including effects owing to metal line cooling is therefore crucial for realistic modelling of galaxy formation because it affects directly the relation between cooling time and dynamical time of forming galaxies. We therefore include a treatment of radiative cooling consistent with the metal content of the gas component produced by the enrichment model. We use the tables computed by SD93 for the metal-dependent cooling functions, and interpolate from them for other metallicities as needed. For particles with iron abundance larger than 0.5, we adopt the suprasolar cooling rate (i.e. that for [Fe/H] > +0.5). In cosmological simulations, we also include a redshift-dependent photo-heating UV background, with an intensity evolution that follows the model of Haardt & Madau (1996).

3 RESULTS FOR ISOLATED GALAXY MODELS

As first tests of our model, we consider simulations of isolated haloes set up to form disc galaxies at their centre. This allows us to examine the dependence of the results on resolution and on different parameters of the chemical enrichment model. The initial conditions consist of a static dark matter potential corresponding to a Navarro, Frenk & White (1996,1997) profile of concentration $c = 20$, and a baryonic gas phase initially in hydrostatic equilibrium in this potential. Our typical system has virial mass $M_{200} = 10^{12}\,h^{-1}{\rm M}_\odot$ ($h = 0.7$), 10 per cent of which is in the form of baryons ($M_{\rm bar} = 10^{11}\,h^{-1}\,{\rm M}_\odot$). The initial radius of the system is $r_{200} = 160\ h^{-1}$ kpc and the gas has an initial angular momentum characterized by a spin parameter $\lambda = 0.1$. We have followed the evolution of this system for 1.5 $\tau_{\rm dyn}$, where $\tau_{\rm dyn} = 7$ Gyr is the dynamical time at r_{200}.

These idealized initial conditions yield a simple model for disc formation, which is an ideal test bench for the performance and validity of the code, and the dependence of the results on the free parameters. We stress however that these models are not meant to provide a realistic scenario for the whole galaxy formation process. Results for full cosmological simulations will be discussed in Section 4, where we analyse the properties of galactic objects formed in Λ cold dark matter (CDM) models with virial masses of $M_{\rm vir} \approx 10^{12}\ h^{-1}\ {\rm M}_\odot$, comparing them also to the results of the idealized tests discussed here.

3.1 Numerical resolution

Both the star formation process and the distribution of metals can be affected by numerical resolution. Particularly important for our model is the fact that the smoothing length of the particles (i.e. the radius which encloses ≈32 gaseous neighbours) determines the region where the newly released chemical elements are injected. Mosconi et al. (2001) found that chemical abundances could be oversmoothed in low-resolution simulations because metals are distributed over a comparatively large volume and, consequently, are more efficiently mixed with surrounding gas. On the other hand, high numerical resolution could also produce spurious results if the metal mixing mechanism becomes too inefficient. Provided other physical mixing mechanisms are not operating, the simulation results might show an artificially large dispersion in gas metallicities.

In order to test the effects of numerical resolution, we carried out simulations of the isolated disc system described above using three different initial numbers of gas particles: 2500 (R1), 10 000 (R2) and 40 000 (R3), with mass resolutions of 4×10^7, 10^7 and $0.25 \times 10^7\,h^{-1}\,{\rm M}_\odot$ for R1, R2 and R3, respectively. We have set the gravitational softening to $0.4\ h^{-1}$ kpc. In these three runs we use metal-dependent cooling functions for the gas particles according to the tables by SD93. In Table 1 we summarize the main characteristics of these simulations.

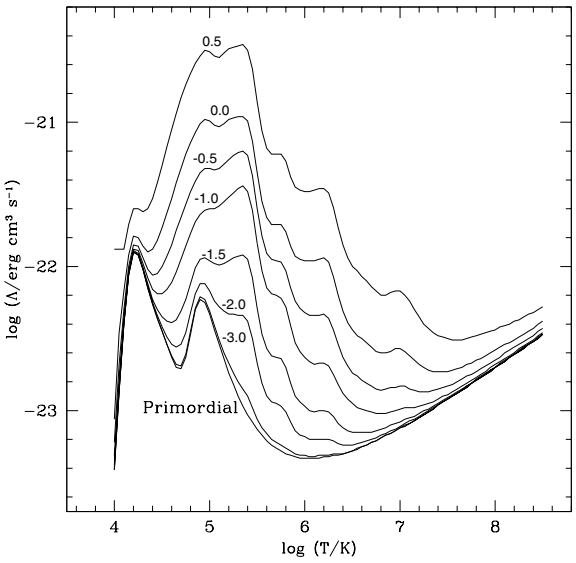

Figure 1. Cooling rates for gas of different metallicities, as given by the [Fe/H] abundance, from suprasolar ([Fe/H] = 0.5) to primordial. The plot is based on data adapted from SD93.

Table 1. Chemical model parameters for the different tests of the idealized isolated galaxy: initial number of gas particles $N_{\rm gas}$, typical lifetimes associated with SNII ($\tau_{\rm SNII}$) and SNIa ($\tau_{\rm SNIa}$) in Gyr, rate of SNIa and cooling functions adopted.

Test	$N_{\rm gas}$	$\tau_{\rm SNII}$	$\tau_{\rm SNIa}$	Rate$_{\rm SNIa}$	Cooling function
R1	2500	0	0.1–1	0.0015	Metal-dependent
R2	10 000	0	0.1–1	0.0015	Metal-dependent
R3	40 000	0	0.1–1	0.0015	Metal-dependent
P1	10 000	0	0.1–1	0.0033	Metal-dependent
P2	10 000	0	0	0.0015	Metal-dependent
P3	10 000	see Section 3.2	0.1−1	0.0015	Metal-dependent
PC	10 000	0	0.1–1	0.0015	Primordial
SC	10 000	0	0.1–1	0.0015	Suprasolar

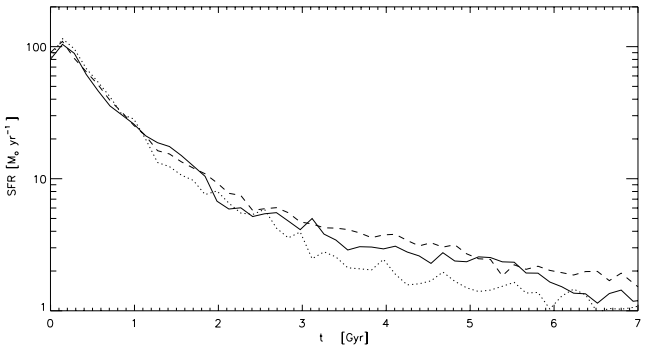

Figure 2. Evolution of the SFR for our test simulations of isolated disc galaxies, as a function of different numerical resolution. R1 (dotted line) has 2500 particles, R2 (solid line) 10 000 particles, and R3 (dashed line) 40 000 particles.

In Fig. 2, we show the evolution of the SFRs obtained for R1 (dotted line), R2 (solid line) and R3 (dashed line). Most of the stellar mass (92, 88 and 86 per cent in R1, R2 and R3, respectively) is formed at times $t < 3$ Gyr (43 per cent of the dynamical time) in the three runs. Only at later times, we find that the lowest resolution test simulation (R1) yields a significantly lower result for the SFR, indicating that the number of gas particles has dropped so much by the conversion into stars that discrete effects become appreciable. However, the final stellar mass fractions (i.e. stellar mass formed divided by the total baryonic mass) are very similar in R1, R2 and R3.

This can be also appreciated from Fig. 3, where we show the mass-weighted metallicity profiles for R1 (dotted line), R2 (solid line) and R3 (dashed line), in the inner region and for the stellar (left column) and gaseous (right column) components and for three different times, $t = 0.13$ Gyr (upper panels), $t = 2.5$ Gyr (middle panels) and $t = 7$ Gyr (lower panels). We can see that the stellar abundance profiles are insensitive to resolution. The mean iron abundance differs by less than 0.03 dex between the different simulations. Recall that the stellar metallicity of newly forming stars is given by the local gas metallicity. This is directly visible at the beginning of the simulation where the gaseous and stellar components show a similar level of enrichment in star-forming regions (upper panels in Fig. 3), while at later stages of the evolution (middle and lower panels) this constraint becomes hidden as a result of the superposition of stars of different ages.

However, as can be seen from the right panels of Fig. 3, the mass-weighted metallicity profiles for the gas components show stronger differences with resolution than their stellar counterparts. At the beginning of the evolution, the profiles of the three test simulations are still very similar, although the enriched gas is more spread in the highest-resolution test. However, the gas profiles differ more at later times when factors such as variations in the consumption time of the gas and differences in the spatial distribution of stars begin to affect the radial distribution of metals. At the end of the simulations (lower-right panel), the mean gaseous iron abundance for R1 is significantly lower than those for the other two simulations. This decrease in the metallicity is produced by the infall of less enriched gas. This gas is not becoming dense enough to trigger star formation activity at the level of R2 and R3, and the infall tends to dilute the metal content in

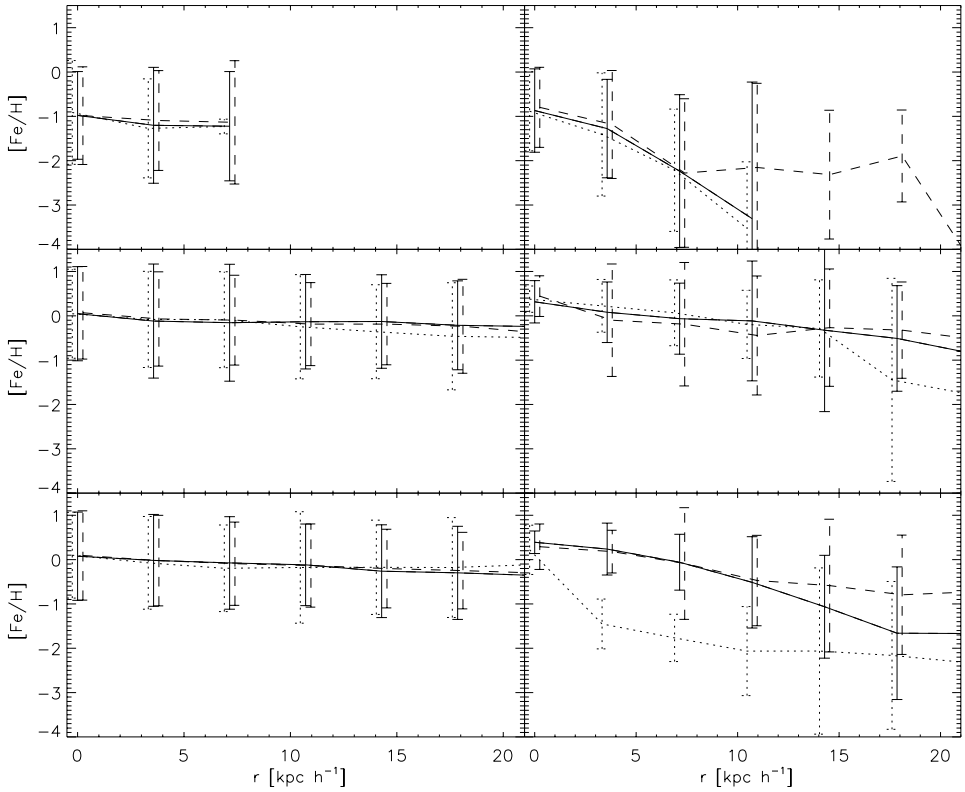

Figure 3. Metallicity profiles for the stellar (left panels) and gaseous (right panels) components of the idealized disc tests performed with different resolution: R1 (dotted line, 2500 particles), R2 (solid line, 10 000 particles) and R3 (dashed line, 40 000 particles). The different rows show different times of the evolution: $t = 0.13$ Gyr (upper panels), $t = 2.5$ Gyr (middle panels) and $t = 7$ Gyr (lower panels). The error bars correspond to the rms scatter of [Fe/H] around the mean in each radial bin.

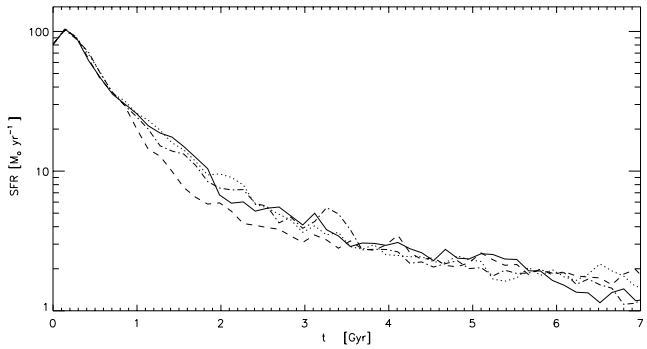

Figure 4. SFR for the experiments of the idealized disc galaxy run with different SN parameters: R2 (solid line, standard test), P1 (dotted line, higher SNIa rate), P2 (dashed line, IRA for SNIa) and P3 (dash-dotted line, relaxing the IRA for SNII).

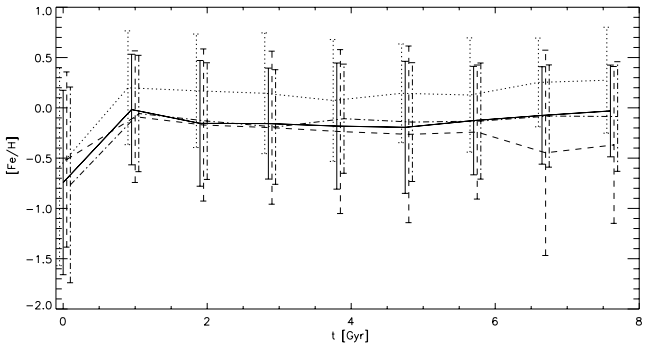

Figure 5. AMR for the stellar component in the tests of the idealized disc galaxy run with different SN parameters: R2 (solid line, standard test), P1 (dotted line, higher SNIa rate), P2 (dashed line, IRA for SNIa) and P3 (dash-dotted line, relaxing the IRA for SNII). The error bars correspond to the rms scatter of [Fe/H] around the mean.

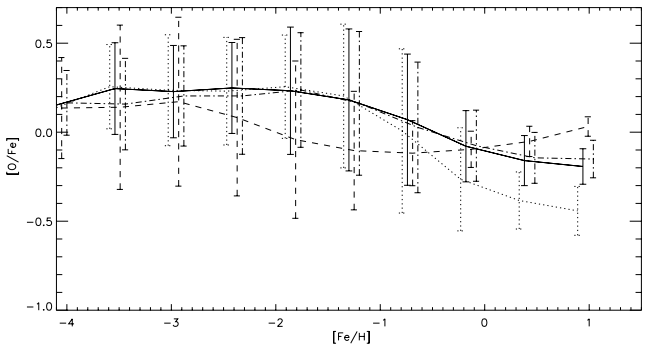

Figure 6. [O/Fe] abundance as a function of [Fe/H] for the stellar component in experiments of the idealized disc galaxy run with different SN parameters: R2 (solid line, standard test), P1 (dotted line, higher SNIa rate), P2 (dashed line, IRA for SNIa) and P3 (dash-dotted line, relaxing the IRA for SNII). The error bars correspond to the rms scatter of [O/Fe] around the mean.

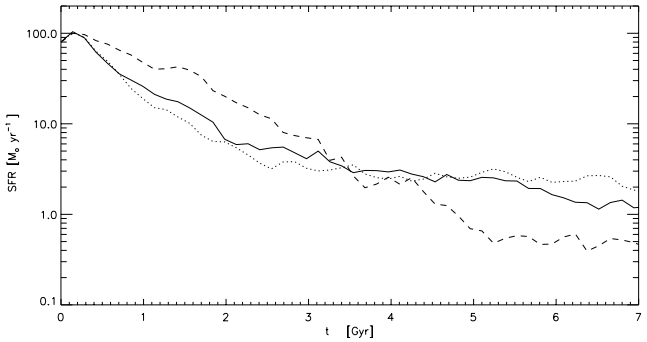

Figure 7. SFR for the idealized disc test run with suprasolar (SC, dashed line), primordial (PC, dotted line) and metal-dependent (R2, solid line) cooling functions.

the ISM. Hence, the fact that the gas component in R1 shows a lower iron abundance is driven by its poorer gas resolution. Note that as a result of the consumption of most of the gas, the final number of gas particles in R1 is very low ($\sim$60 in the inner 30 kpc) and, as a consequence, the distribution of metals in the gas component is strongly affected by numerical noise. On the other hand, the results for the tests with 10 000 and 40 000 particles converge quite well both in their stellar and gaseous chemical properties. Note that the rms scatter of particles within each radial bin is similar for the different tests indicating that, on average, the metal mixing is not significantly affected by resolution if we consider at least an initial number of particles of 2500 or more.

3.2 Dependence on assumed supernova characteristics

In this section we analyse the dependence of our results on important input parameters of the chemical model, namely the IRA for SNII, and the rate and lifetimes associated with SNIa. For this purpose we run three additional test simulations. In runs P1 and P2, we change the SNIa parameters compared with the simulation R2, which we take as a fiducial reference model, while in run P3 we release the IRA condition for SNII. The main characteristics of these simulations are listed in Table 1.

In Fig. 4, we compare the evolution of the SFR of the standard R2 run (solid line) with P1 (dotted line), in which the SNIa rate was increased. We find no significant differences between the SFRs of these tests. However, we find a larger difference in their stellar age–metallicity relations (AMR), as seen in Fig. 5, although the results appear consistent within the standard deviation based on counting statistics. In this plot, an increase in the SNIa rate translates into a shift towards larger values of stellar metallicities, because the ISM is more strongly enriched by heavy elements. A change of the SNIa rate also impacts other chemical properties of the systems. For example, in Fig. 6 we show the [O/Fe] abundance as a function of [Fe/H] for stars in R2 and P1 at $\tau_{\rm dyn}$. The main difference is found for the high-metallicity material ([Fe/H] > -0.5) which shows in P1 a lower α-enhancement compared to that in R2, as expected.

We have also tested the sensitivity of the results on the lifetime of binary systems associated with SNIa. The importance of including SNIa has been previously pointed out by Greggio & Renzini (1983) and Mosconi et al. (2001), among others. Motivated by these previous results, we carried out a simulation P2 where we assumed an IRA for SNIa explosions (see Table 1). The main effect of instantaneously releasing the chemical production of SNIa can be appreciated from Fig. 6, which shows the mean α-enhancement of the simulated stellar population. These abundance ratios exhibit a behaviour which is in open disagreement with observations (Pagel 1997). Note, however, that these observational results correspond to solar neighbour stars, while the simulated results include information from the whole stellar component.

Finally, in order to analyse the effects of the IRA for SNII, we tested a more detailed calculation of the lifetime of massive stars. To

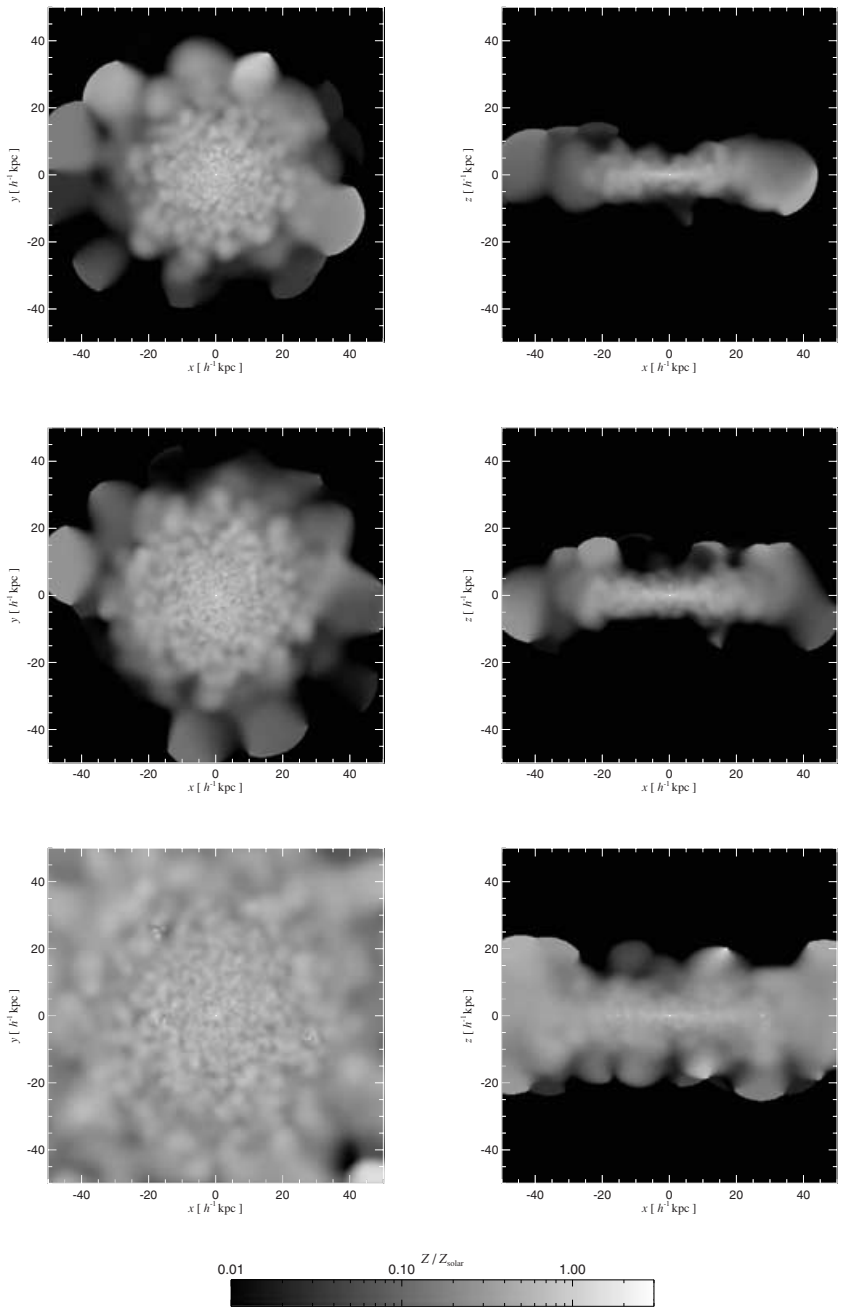

Figure 8. Face-on (left-hand panels) and edge-on (right-hand panels) surface metallicity distribution for the stellar component of the isolated disc galaxy tests run with primordial (PC, upper row), metal-dependent (R2, middle row) and suprasolar (SC, lower row) cooling rate functions. The metallicity scale is also shown.

this end, we convolved the IMF with the lifetime of massive stars at different intervals of metallicity (Raiteri, Villata & Navarro 1996). In this way, we obtained a range of mean lifetimes varying with stellar metallicity from 6.3×10^6 yr for $Z = 5 \times 10^{-4}\ Z_\odot$ to 1.6×10^7 yr for $Z = Z_\odot$, where Z denotes mean stellar metallicity and $Z_\odot$ is the solar metallicity. We run a test of our idealized initial condition with the same chemical parameters used in R2 but including these metallicity-dependent lifetimes for SNII (P3, see Table 1). We found no significant differences between the two tests, either in the SFR or in the iron abundance, as can be seen from Figs 4 and 5. The similar behaviour of these two runs is also found in other chemical properties of the systems, such as the relation shown in Fig. 6. Recall that a drawback of a detailed description of chemical enrichment can be its high computational cost, so an important practical goal is to keep the model sufficiently simple to allow its use in large-scale cosmological simulations. While in this context the IRA for SNIa in general cannot reproduce certain observed trends, for SNII it appears to be a simple and sufficiently accurate simplification, at least for these simple tests that do not include energy feedback.

3.3 Effects of metal-dependent cooling

Finally, we performed two more runs of our idealized isolated galaxy in order to highlight effects owing to a metal-dependent cooling

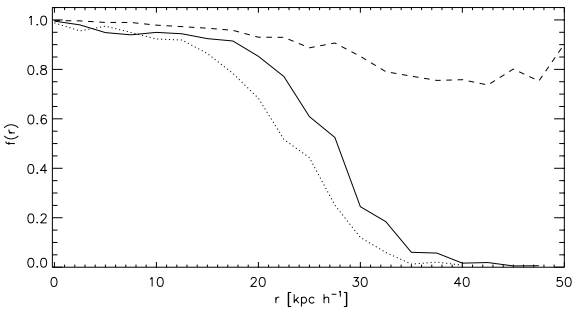

Figure 9. Fraction of baryons in stellar form $f(r)$ for the idealized disc tests run with suprasolar (SC, dashed line), primordial (PC, dotted line) and metal-dependent (R2, solid line) cooling functions.

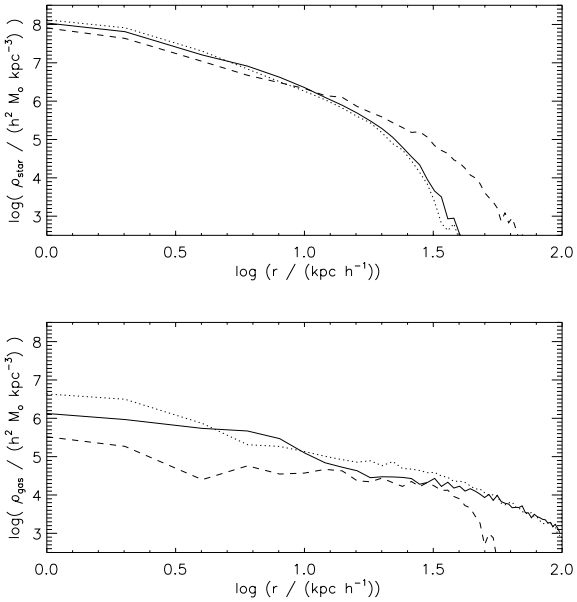

Figure 10. Density profiles for the stellar (upper panel) and gaseous (lower panel) components for the idealized disc tests run with suprasolar (SC, dashed line), primordial (PC, dotted line) and metal-dependent (R2, solid line) cooling functions.

function. In these fiducial tests, we assumed a constant metallicity, either primordial (PC) or suprasolar (SC, [Fe/H] = +0.5) for the cooling function. The parameters for star formation and SN rates were the same as in the standard simulation R2 discussed earlier (see Table 1).

In Fig. 7, we compare the evolution of the SFR for R2 (solid line), PC (dotted line) and SC (dashed line). In the early stages ($t \leqslant 4$ Gyr), the test run with suprasolar abundance cooling function (SC) results in a SFR higher by up to a factor of 3 compared with the simulation R2 with self-consistent cooling function, while the run PC with primordial cooling lies lower by up to a factor 1.5. After the first 4 Gyr, the SFR in the SC run decreases significantly, indicating that most of the gas has already been consumed and transformed into stars. Likewise, after this period, simulation PC has the highest residual level of SFR as a result of the larger amount of gas left over and available for star formation.

As a result of the differences in the level of star formation activity among the runs with different cooling functions, the metallicity distribution is also affected. In Fig. 8 we show metallicity maps for the stellar components corresponding to face-on (left panels) and edge-on (right panels) projections of the discs, for the PC (upper panel), R2 (middle panel) and SC (lower panel) simulations. Comparing the upper to the lower panels, the distribution of stars is more extended and the level of enrichment is higher in the SC run. In fact, the increase in the cooling efficiency produces an increase in the star formation activity at larger radius, increasing the amount of metals and affecting their relative distribution. This can also be appreciated from Fig. 9, which shows the fraction of baryons in stellar form $f(r)$ as a function of radius for tests R2 (solid line), PC (dotted line) and SC (dashed line) at $\tau_{\rm dyn}$. These fractions were calculated by summing up the stellar mass in radial bins, normalized to the total baryonic mass within the corresponding bin. In particular, at $20\,h^{-1}$ kpc the distribution functions for R2 and SC are, respectively, 25 and 35 per cent higher than that for the PC run. Note that the impact of using different cooling functions becomes more important as we go to outer regions where, in the limiting case of SC, the high cooling efficiency leads to a substantial star formation activity even outside $30\,h^{-1}$ kpc. The behaviour found in this figure is present already in the early stages of the evolution. The efficient transformation of gas into stars at larger radius also limits the supply of baryons to inner regions. Hence, the whole mass distribution is affected by the use of different cooling functions. This is clear from Fig. 10, where we show the density profiles of the stellar (upper panel) and gaseous (lower panel) components for these tests.

Finally, in Fig. 11 we show the mass-weighted oxygen profiles for the stellar (left panels) and gaseous (right panels) components for the tests PC (dotted line), R2 (solid line) and SC (dashed line), at three different times: $t = 0.13$ Gyr (upper panels), $t = 2.5$ Gyr (middle panels), $t = 7$ Gyr (lower panels). We find no significant differences in the abundance distributions for the stars in these tests at any time. However, the metallicity of the gaseous component is more sensitive to the adopted cooling functions. At the beginning of the simulations, the results for the three runs are similar but after the initial collapse (middle panel) the level of enrichment increases from PC to R2 and SC, even though the differences remain quite small overall. At $\tau_{\rm dyn}$ (lower panel), both the PC and R2 simulations show decreasing metallicity profiles, conversely to the case of SC which shows a flat relation. Here metals are more uniformly distributed and the ISM is enriched out to larger radii. Recall that the gas metallicities reflect an instantaneous state of the chemical properties of the system, while the stellar population gives an integrated account of the history of the chemical properties of the galaxy.

In summary, the results of this section show that a detailed study of the metallicity properties of galaxies requires a self-consistent treatment of radiative cooling that accounts for metal line cooling. The resulting effects will, however, depend strongly on how heavy elements are spread into diffuse unenriched gas.

4 RESULTS FOR COSMOLOGICAL SIMULATIONS

We here discuss first results for full cosmological simulations of the hierarchical growth of galaxies, allowing us to more realistically assess the effects of chemical enrichment on galaxy properties. To this end, we have run a cosmological simulation (C2) in a CDM universe with cosmological parameters $\Omega_{\rm m} = 0.3$, $\Omega_\Lambda = 0.7$, $\Omega_{\rm b} = 0.04$, $H_0 = 100\,h^{-1}$ km s^{-1} Mpc^{-1}, $h = 0.7$ and $\sigma_8 = 0.9$. We used a periodic simulation box of $10\,h^{-1}$ Mpc on a side, populated initially with $N = 2 \times 80^3$ particles, which yields an initial mass resolution of $\approx 1.4 \times 10^8$ and $\approx 2.16 \times 10^7\,h^{-1}$ M$_\odot$ for dark matter and gas particles, respectively. We have adopted a maximum gravitational softening of $5\,h^{-1}$ kpc for dark matter, gas and star particles. We

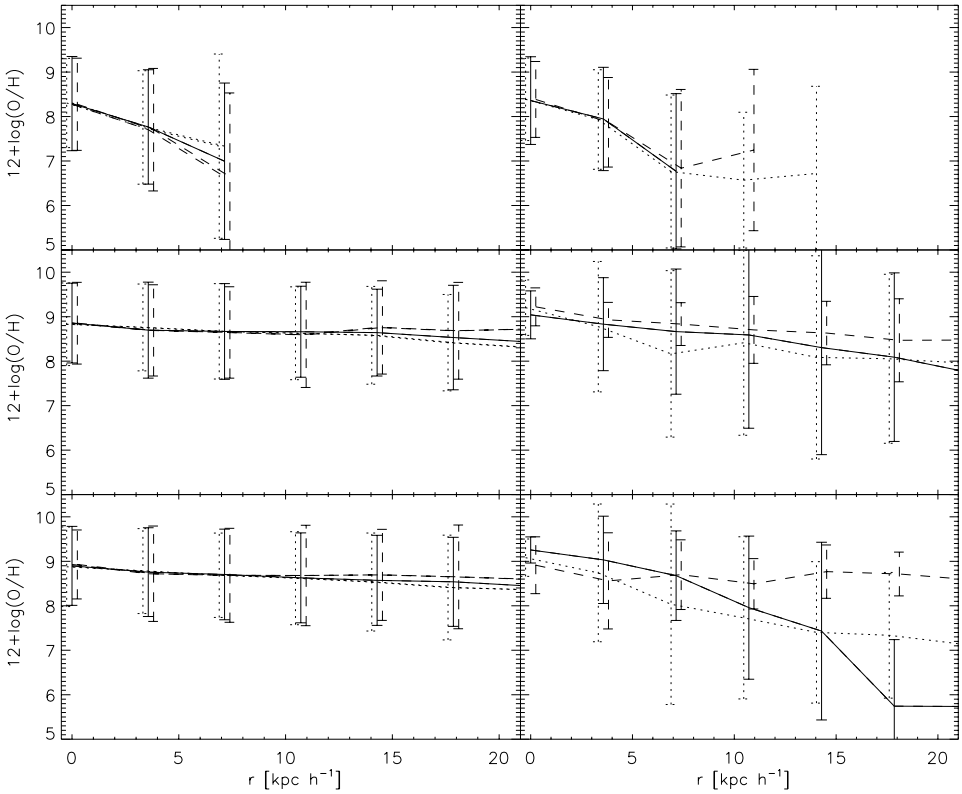

Figure 11. Oxygen profiles for the stellar (left panel) and gaseous (right panel) components in experiments of the idealized disc galaxy run with different cooling functions: R2 (solid line, metal-dependent cooling), PC (dotted line, cooling function for primordial abundance) and SC (dashed line, cooling function for suprasolar abundance). The error bars correspond to the rms scatter of 12 +log (O/H) around the mean.

Table 2. Chemical model parameters for the cosmological tests: initial number of gas and dark matter particles $N_{\rm gas}$ and $N_{\rm DM}$, typical lifetimes associated with SNII ($\tau_{\rm SNII}$) and SNIa ($\tau_{\rm SNIa}$) in Gyr, rate of SNIa and cooling functions adopted.

Test	$N_{\rm gas} = N_{\rm DM}$	$\tau_{\rm SNII}$	$\tau_{\rm SNIa}$	Rate$_{\rm SNIa}$	Cooling function
C1	512 000	0	0.1–5	0.0015	Primordial
C2	512 000	0	0.1–5	0.0015	Metal-dependent
C3	512 000	0	0.1–5	0.0015	Suprasolar

used a metal-dependent, self-consistent cooling function for the gas component. Table 2 summarizes the main characteristics of this run.

In order to test the dependence of our results on mixing processes and metal-dependent cooling, we have also carried out two additional runs with the same parameters, but a constant metallicity for the cooling function. As a limiting case of a very enriched medium, in simulation C3 we used suprasolar abundance (see Table 2), while in simulation C1 we took primordial cooling in order to model a situation where mixing processes are completely absent. These two cases should hence bracket reality.

In our cosmological simulations, we identified galactic objects at $z = 0$ as virialized structures using a density-contrast criterion with overdensity $\delta\rho/\rho \approx 178\Omega_0^{-0.6}$ (White, Efstathiou & Frenk 1993). In our analysis we focus on six haloes with masses similar to the idealized disc test R2 ($\simeq 10^{12}$ M$_\odot$). They are resolved with a similar or higher number of particles ($N \geqslant 10\,000$; see Table 3). Note that as gas/star particles do not have the same mass, the number of particles in these components does not, however, trace the mass. The main properties of these objects are given in Table 4.

In Fig. 12, we compare the star formation histories for the selected galactic objects in C1 (dotted line), C2 (solid line) and C3 (dashed line), as a function of look-back time, i.e. $\tau(z) = 1 - (1 + z)^{-3/2}$. Note that the global features of the SFRs are preserved in the three runs, although the detailed levels of activity are different. In general, the SFRs of the galactic objects formed in C3 are systematically higher than the corresponding ones in C2, as expected. Note that because galactic objects formed in C3 have higher SFRs than those in C2, their final stellar masses are much larger than the corresponding ones in C2 (see Table 4). If we compare the SFRs obtained for C1 and C2, although the differences are small, the SFRs in C1 are systematically lower than those in C2. It is noteworthy that the impact of metallicity on the star formation history seems to depend on the particular evolutionary histories of the systems, as can be appreciated from Fig. 12.

In Fig. 13, we show the mean stellar mass fraction $\langle f(r)\rangle$ as a function of radius, estimated from the six selected galactic objects in C1 (dotted line), C2 (solid line) and C3 (dashed line). As in Section 3.3, the distribution function for each galactic object was calculated by summing up the stellar mass in bins of radius normalized to the total baryonic mass within the corresponding bin. As we found for the tests of the isolated galaxies, there are clear differences between the results for the three runs. Although in the inner $10\,h^{-1}$ kpc the simulations yield similar stellar fractions, within $40\,h^{-1}$ kpc, galactic objects in C2 have transformed a larger fraction of the gas into stars compared with those in C3, while galactic objects in C1 show the opposite behaviour. At larger radii, the mean distribution function of stellar mass for the galactic objects in C3 is significantly larger than its counterpart for C2, indicating that as a result of the higher cooling efficiency, the gas in C3 has been transformed

Table 3. Number of dark matter ($N_{\rm DM}$), gas ($N_{\rm gas}$) and stars ($N_{\rm star}$) within the virial radius for the six galactic objects (GLOs) identified in the cosmological tests run with primordial (C1), metal-dependent (C2) and suprasolar (C3) cooling functions.

	C1			C2			C3		
GLO	$N_{\rm DM}$	$N_{\rm gas}$	$N_{\rm star}$	$N_{\rm DM}$	$N_{\rm gas}$	$N_{\rm star}$	$N_{\rm DM}$	$N_{\rm gas}$	$N_{\rm star}$
1	8591	2149	12 838	8552	1881	13 382	8739	1486	19 368
2	5454	1337	7573	5482	1270	8013	5684	1431	12 313
3	21 816	8947	24 218	21 790	6930	27 105	22 275	2442	43 430
4	5738	1858	7785	5656	1740	8240	5840	1569	11 956
5	8738	2724	12 385	8688	2451	13 362	8934	1736	20 465
6	4980	1506	7868	4966	1476	8166	5150	1512	10 482

Table 4. Virial mass ($M_{\rm vir}$), stellar mass ($M_{\rm star}$, both in $10^{10}\ h^{-1}\ {\rm M}_{\odot}$) and optical radius ($r_{\rm opt}$ in h^{-1} kpc) for the six galactic objects (GLOs) identified in the cosmological tests run with primordial (C1), metal-dependent (C2) and suprasolar (C3) cooling functions.

	C1			C2			C3		
GLO	$M_{\rm vir}$	$M_{\rm star}$	$r_{\rm opt}$	$M_{\rm vir}$	$M_{\rm star}$	$r_{\rm opt}$	$M_{\rm vir}$	$M_{\rm star}$	$r_{\rm opt}$
1	139.28	13.74	15.05	138.81	14.35	14.20	146.70	20.72	15.70
2	87.79	8.11	15.38	88.52	8.58	14.15	95.98	13.16	14.99
3	352.44	25.91	13.31	351.07	29.06	12.51	365.50	46.56	12.40
4	93.04	8.32	14.30	92.09	8.79	13.47	98.26	12.80	12.73
5	142.10	13.26	12.06	141.79	14.30	11.78	151.09	21.89	10.90
6	81.63	8.40	12.38	81.70	8.72	12.58	86.71	11.20	14.71

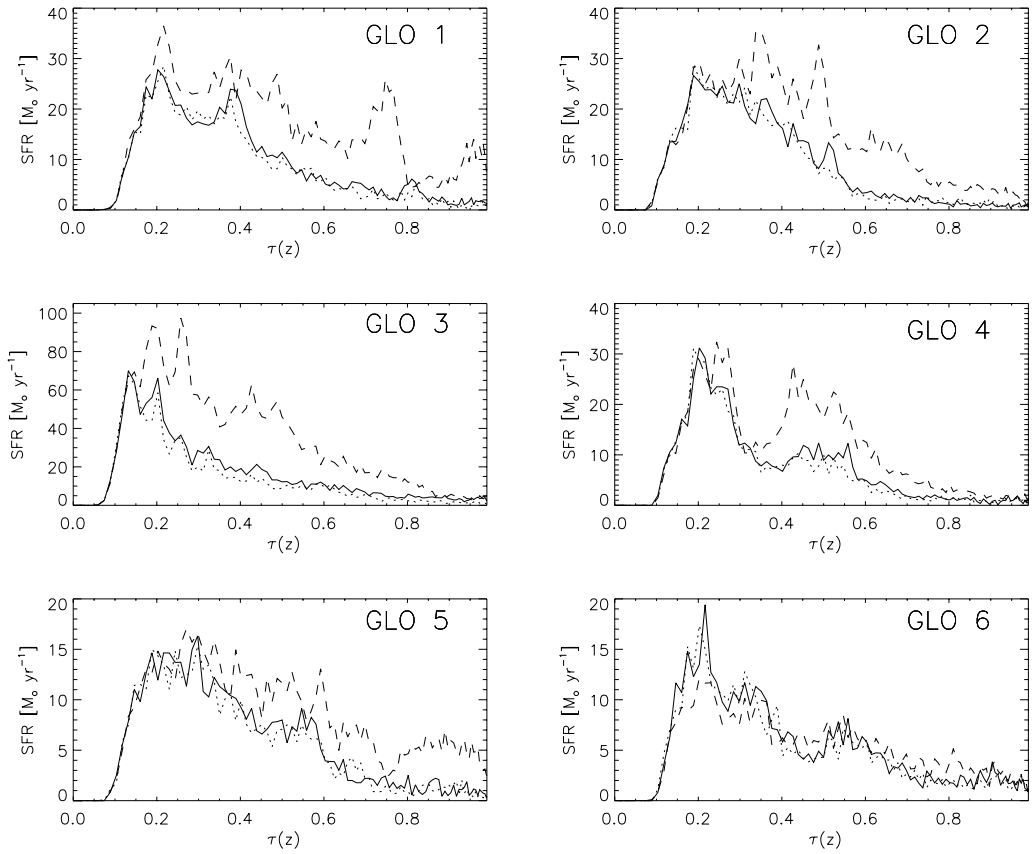

Figure 12. SFR for the six selected galactic objects from the cosmological simulations run with primordial (dotted line), metal-dependent (solid line) and suprasolar (dashed lines) cooling functions.

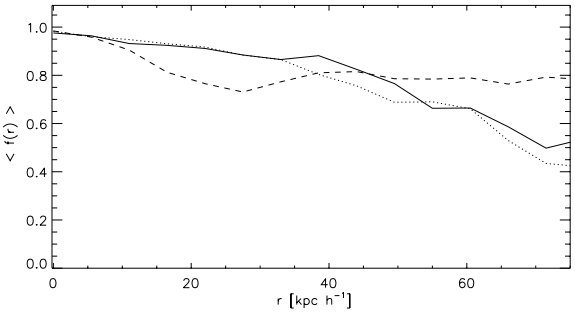

Figure 13. Mean stellar mass fraction as a function of radius for the six selected objects in the cosmological simulations run with primordial (C1, dotted line), metal-dependent (C2, solid line) and suprasolar (C3, dashed line) cooling functions as a function of radius.

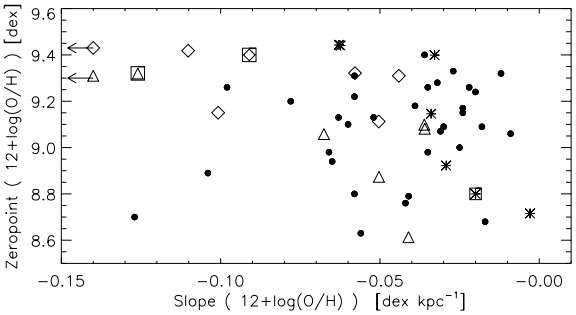

Figure 15. Zero-point of the relation $12 + \log(\mathrm{O/H})$ for the gas components of the selected galactic objects from the cosmological simulations as a function of the corresponding slopes. We have included results from primordial (triangles), metal-dependent (diamonds) and suprasolar (asterisks) cooling functions. For comparison, results for the tests of the isolated disc galaxy run with primordial (squared triangle), metal-dependent (squared diamond) and suprasolar (squared asterisk) cooling functions are also shown. We have also included observations from Zaritsky et al. (1994, filled circles). The diamond and the triangle with the arrows have slopes of -0.24 and -0.23, respectively.

into stars further away from the centre of mass of the objects. Conversely, the primordial run shows fewer stars in the outer region. Note that efficient energy feedback is needed to prevent excessive star formation in the outer regions, as can be observed from Fig. 13.

In order to assess how these differences affect the chemical properties of the formed galactic objects, we analysed the metal indicator $12 + \log(\mathrm{O/H})$ for the gaseous and stellar components in C1, C2 and C3. Consistent with our results for the idealized disc tests, we found that the metallicity of the stellar components is not sensitive to the cooling function adopted, in contrast to the gaseous components. In Fig. 14 we compare the gaseous oxygen profiles for the galaxy samples in C1 (dotted lines), C2 (solid lines) and C3 (dashed lines). Although there is a trend for systems in C3 to have a higher level of enrichment and flatter mass-weighted abundance profiles compared to their counterparts in C2 and C1, how much metals affect these relations seems to depend on the particular history of evolution of each galaxy, as can be inferred from Figs 12 and 14.

Finally, for a comparison with observational results, we performed linear regression fits to the gaseous oxygen profiles of our simulated galactic objects within the optical radius. By definition, the optical radius encloses 83 per cent of the baryonic stellar mass

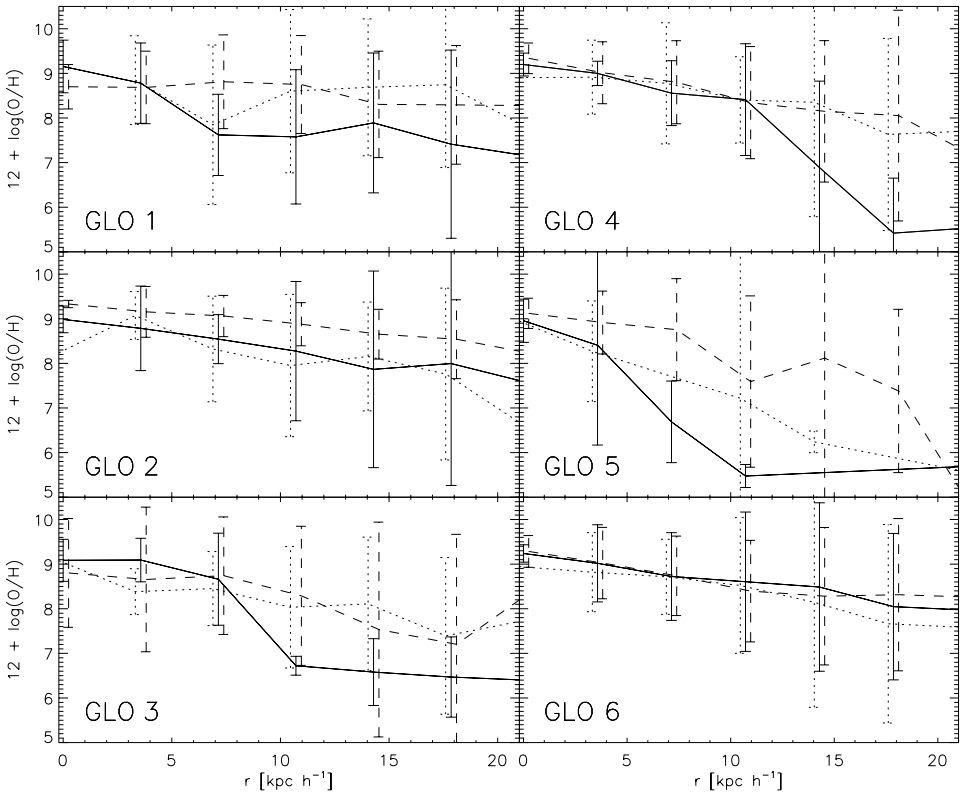

Figure 14. Oxygen profiles for the gaseous components of the six selected galactic objects from the cosmological simulations run with primordial (dotted lines), metal-dependent (solid lines) and suprasolar (dashed lines) cooling functions. The error bars correspond to the rms scatter of $12 + \log(\mathrm{O/H})$ around the mean.

within the virial radius. In Fig. 15, we show the zero-point of these fits as a function of the corresponding slopes for the galactic objects in C1 (triangles), C2 (diamonds) and C3 (asterisks). We also include observational results from Zaritsky et al. (1994, filled circles). In general, the properties of the simulated galactic objects agree reasonably well with the range obtained in observational studies. However, the simulated galactic objects identified in C2 tend to have steeper profiles and higher zero-points compared with observations. Conversely, galactic objects in C3 exhibit flatter profiles. A similar behaviour was also found in our tests for the isolated disc galaxies run with primordial (PC, squared triangle), metal-dependent (R2, squared diamond) and suprasolar (SC, squared asterisk) cooling functions. The fact that these simulations do not reproduce the whole observed range of gradients could be related to the lack of a treatment of energy feedback by SNe. The latter, if realistically modelled, is expected to trigger mass outflows from the star-forming regions into the halo. Because these regions are highly enriched, metals may be transported outwards, affecting the metallicity distributions and flattening the metallicity profiles. Our simulation run with suprasolar cooling function was performed in order to assess the effects of the presence of metals in these outer regions on the gas cooling, mimicking an extreme case of metal enrichment by energy feedback.

5 CONCLUSIONS

We have implemented a new model for chemical evolution within the cosmological SPH code GADGET-2. We account for nucleosynthesis from SNIa and SNII separately. Radiative cooling of the gas according to self-consistent metallicity values is realized by means of pre-computed look-up tables. Our implementation was designed to allow a reasonably accurate treatment of the main features of stellar evolution while still not becoming computationally too expensive.

Using a number of test simulations, both of isolated galaxies and of cosmological structure formation, we have validated our implementation and established some first basic results for the effects of chemical enrichment. An important consequence of the presence of metals is the increase in the cooling efficiency that it can cause, leading to accelerated star formation. In our isolated galaxy simulations, the SFR for test runs with metal-dependent cooling function can be up to a factor of 1.5 higher than the corresponding one for a test with a primordial cooling function, and up to a factor of 3 lower than that for suprasolar cooling. We found that these differences do not originate in the gas in the central regions, because it is already cold and dense anyway. Instead, the differences are caused by more diffuse gas at outer radii which has yet to cool. Here the increase of the cooling efficiency allows condensation of gas and star formation to occur further away from the centre of the systems.

An important implication of this result is that strong effects owing to metal-dependent cooling can only be expected when heavy elements are efficiently transported and mixed into diffuse gas that has yet to cool. In our cosmological simulations, which lacked a physical model for energy feedback, such a large-scale spreading of metals only occurs at a low level. As perhaps was to be expected, we found that simulations with metal-dependent cooling produced similar results as simulations with a primordial cooling function. We expect however that this could be very different if a model for efficient metal distribution is added to our simulations. An explicit demonstration of this has been provided by our test simulation where we assumed suprasolar cooling rate functions, resulting in substantially elevated star formation activity and different abundance profiles. Note that in this paper we have explored galaxy scale systems which cool very efficiently. Larger effects from chemical mixing are expected in more massive haloes such as clusters of galaxies (White & Frenk 1991; De Lucia, Kauffmann & White 2004).

We have also tested the impact of a number of assumptions made in our model, and the relevance of numerical parameters. Relaxing the IRA for SNII has only a negligible effect and does not change the chemical properties of the simulated systems. However, as also shown by previous work (e.g. Raiteri et al. 1996; Chiappini et al. 1997; Mosconi et al. 2001), the chemical properties of both the stellar populations and the ISM are sensitive to the time delay associated with SNIa explosions. In agreement with previous results, we found that the latter must be included in order to be able to reproduce the observed chemical properties of galaxies.

We have shown that chemical enrichment can significantly modify the chemical and dynamical properties of forming galactic systems. However, the strength of the influence of metals on galaxy formation might also depend on the physics of energy feedback. If the latter is neglected, as we have done here, metals are not mixed widely in gas that has yet to cool. Effects due to metal-dependent cooling remain then moderate. In a forthcoming paper, we will complement our model for chemical enrichment with a new description of a multiphase ISM and energy feedback, which is capable of reproducing strong outflows and regulating the star formation activity. This combined model should provide a powerful tool to exploit observational data on the chemical properties of galaxies to constrain galaxy formation.

ACKNOWLEDGMENTS

We thank the anonymous referee for comments that helped to improve the paper. This work was partially supported by the European Union's ALFA-II programme, through LENAC, the Latin American European Network for Astrophysics and Cosmology. Simulations have been performed on the Ingeld PC-Cluster funded by Fundación Antorchas. We acknowledge support from Consejo Nacional de Investigaciones Científicas y Técnicas, Agencia de Promoción de Ciencia y Tecnología, Fundación Antorchas, Secretaría de Ciencia y Técnica de la Universidad Nacional de Córdoba and the DAAD Exchange programme. CS thanks the Alexander von Humboldt Foundation, the Federal Ministry of Education and Research and the Programme for Investment in the Future (ZIP) of the German Government for partial support.

REFERENCES

Abadi M. G., Navarro J. F., Steinmetz M., Eke V. R., 2003, ApJ, 591, 499
Adelberger K. L., Steidel C. C., Shapley A. E., Pettini M., 2003, ApJ, 584, 45
Boisser S., Prantzos N., 2000, MNRAS, 312, 398
Brodie J. P., Huchra J. P., 1991, ApJ, 379, 157
Burkert A., Hensler G., 1988, A&A, 199, 131
Burkert A., Truran J. W., Hensler G., 1992, ApJ, 391, 651
Chiappini C., Matteucci F., Gratton R., 1997, ApJ, 477, 765
Dahlem M., Weaver K. A., Heckman T. M., 1998, ApJS, 118, 401
De Lucia G., Kauffmann G., White S. D. M., 2004, MNRAS, 349, 1101
Dekel A., Silk J., 1986, ApJ, 303, 39
Domínguez-Tenreiro R., Tissera P. B., Sáiz A., 1998, ApJ, 508, L123
Ettori S., Fabian A. C., Allen S. W., Johnstone M. N., 2002, MNRAS, 331, 635
Ferrini F., Matteucci F., Pardi C., Peuco U., 1992, ApJ, 387, 138
Frye B., Broadhurst T., Benítez N., 2002, ApJ, 568, 558
Garnett D. R., Shields G. A., 1987, ApJ, 317, 82

Gingold R. A., Monaghan J. J., 1977, MNRAS, 181, 375
Greggio L., 1996, in Kunth D., Guiderdoni B., Heydari-Malayeri M., Thuan T., eds, The Interplay Between Massive Star Formation, the ISM and Galaxy Evolution. Editions Frontières, Gif-sur-Yvette, p. 89
Greggio L., Renzini A., 1983, A&A, 118, 217
Haardt F., Madau P., 1996, ApJ, 461, 20
Kaellander D., Hultman J., 1998, A&A, 333, 399
Kauffmann G., 1996, MNRAS, 281, 475
Kauffmann G., Charlot S., 1998, MNRAS, 294, 705
Kawata D., Gibson B. K., 2003, MNRAS, 340, 908
Kay S. T., Pearce F. R., Jenkins A., Frenk C. S., White S. D. M., Thomas P. A., Couchman H. M. P., 2000, MNRAS, 316, 374
Kobulnicky H. A. et al., 2003, ApJ, 599, 1006
Lamareille F., Mouhcine M., Contini T., Lewis I., Maddox S., 2004, MNRAS, 350, 396
Larson R. B., 1974, MNRAS, 169, 229
Larson R. B., 1976, MNRAS, 176, 31
Lehnert M. D., Heckman T. M., 1996, ApJ, 472, 546
Lia C., Portinari L., Carraro G., 2002, MNRAS, 330, 821
Lilly S. J., Carollo C. M., Stockton A. N., 2003, ApJ, 597, 730
Lucy L. B., 1977, ApJ, 82, 1013
Marri S., White S. D. M., 2003, MNRAS, 345, 561
Martin C. L., 2004, AAS, 205, 8901
Metzler C., Evrard A., 1994, ApJ, 437, 564
Mosconi M. B., Tissera P. B., Lambas D. G., Cora S. A., 2001, MNRAS, 325, 34
Mushotzky R. F., Loewenstein M., Arnaud K., Tamura T., Fukazawa Y., Matsushita K., Kikuchi K., Hatsukade I., 1996, ApJ, 466, 686
Navarro J. F., Benz W., 1991, ApJ, 380, 320
Navarro J. F., White S. D. M., 1993, MNRAS, 265, 271
Navarro J. F., White S. D. M., 1994, MNRAS, 267, 401
Navarro J. F., Frenk C. S., White S. D. M., 1996, ApJ, 462, 563
Navarro J. F., Frenk C. S., White S. D. M., 1997, ApJ, 490, 493
Okamoto T., Eke V. R., Frenk C. S., Jenkins A., 2005, MNRAS, in press (astro-ph/0503676)
Pagel B. E. J., 1997, Nucleosynthesis and Chemical Evolution of Galaxies. Cambridge Univ. Press, Cambridge, chap. 8
Pearce F. R. et al., 1999, ApJ, 521, 99
Pearce F. R., Jenkins A., Frenk C. S., White S. D. M., Thomas P. A., Couchman H. M. P., Peacock J. A., Efstathiou G., 2001, MNRAS, 326, 649
Prochaska J. X., Wolfe A. M., 2002, ApJ, 566, 68
Raiteri C. M., Villata M., Navarro J. F., 1996, A&A, 315, 105
Robertson B., Yoshida N., Springel V., Hernquist L., 2004, ApJ, 606, 32
Rupke D. S., Veilleux S., Sanders D. B., 2002, ApJ, 570, 588
Shapley A. E., Erb D. K., Pettini M., Steidel C. C., Adelberger K. L., 2004, ApJ, 612, 122
Skillman E. D., Kennicutt R. C., Hodge P. W., 1989, ApJ, 347, 875
Springel V., Hernquist L., 2002, MNRAS, 333, 649
Springel V., Hernquist L., 2003, MNRAS, 339, 289 (SH03)
Springel V., Yoshida N., White S. D. M., 2001, NewA, 6, 79
Steinmetz M., Müller E., 1994, A&A, 281, L97
Sutherland R. S., Dopita M. A., 1993, ApJS, 88, 253 (SD93)
Theis C., Burkert A., Hensler G., 1992, A&A, 265, 465
Thielemann F. K., Nomoto K., Hashimoto M., 1993, in Prantzos N., Vangoni-Flam E., Cassé N., eds, Origin and Evolution of the Elements. Cambridge Univ. Press, Cambridge, p. 299
Timmes F. X., Woosley S. E., Weaver T. A., 1995, ApJS, 98, 617
Tinsley B. M., Larson R. B., 1979, MNRAS, 186, 503
Tornatore L., Borgani S., Matteucci F., Recchi S., Tozzi P., 2004, MNRAS, 349, L19
Tremonti C. A. et al., 2004, ApJ, 613, 898
Valdarnini R., 2003, MNRAS, 339, 1117
van den Bergh S., 1991, ApJ, 369, 1
White S. D. M., Frenk C. S., 1991, ApJ, 379, 52
White S. D. M., Rees M. J., 1978, MNRAS, 183, 341
White S. D. M., Efstathiou G., Frenk C. S., 1993, MNRAS, 262, 1023
Woosley S. E., Weaver T. A., 1995, ApJS, 101, 181
Yepes G., Kates R., Khokhlov A., Klypin A., 1997, MNRAS, 284, 235
Zaritsky D., Kennicutt R. C. Jr, Huchra J. P., 1994, ApJ, 420, 87

This paper has been typeset from a TEX/LATEX file prepared by the author.